Technical Note: Measuring tropospheric OH and HO2 by laser-induced fluorescence at low pressure? a comparison of calibration techniques

S. Dusanter, D. Vimal, P. S. Stevens

Atmos. Chem. Phys. Discuss., 7, 12877–12926, 2007
www.atmos-chem-phys-discuss.net/7/12877/2007/

Atmospheric Chemistry and Physics Discussions

Technical Note: Measuring tropospheric OH and HO_2 by laser-induced fluorescence at low pressure – a comparison of calibration techniques

S. Dusanter, D. Vimal, and P. S. Stevens

Center for Research in Environmental Science, School of Public and Environmental Affairs, and Department of Chemistry, Indiana University, Bloomington, Indiana

Received: 16 August 2007 – Accepted: 16 August 2007 – Published: 4 September 2007

Correspondence to: S. Dusanter (sdusante@indiana.edu)

Abstract

The hydroxyl radical (OH) is one of the most important oxidants in the atmosphere, as it is involved in many reactions that affect regional air quality and global climate change. Because of its high reactivity, measurements of OH radical concentrations in the atmosphere are difficult, and often require careful calibrations that rely on the production of a known concentration of OH at atmospheric pressure. The Indiana University OH instrument, based on the Fluorescence Assay by Gas Expansion technique (FAGE), has been calibrated in the laboratory using two different approaches: the production of OH from the UV-photolysis of water-vapor, and the steady-state production of OH from the reaction of ozone with alkenes. Both techniques are shown to agree within their experimental uncertainties, although the sensitivities derived from the ozone-alkene technique were systematically lower than those derived from the water-vapor UV-photolysis technique. The agreement between the two different methods improves the confidence of the water-vapor photolysis method as an accurate calibration technique for HO_x instruments. Because several aspects of the mechanism of the gas phase ozonolysis of alkenes are still uncertain, this technique should be used with caution to calibrate OH instruments.

1 Introduction

The hydroxyl radical (OH) has long been recognized as one of the most important species in atmospheric chemistry (Levy, 1972; Crutzen, 1973). Reactions with OH are the primary removal process for many atmospheric trace gases that are important to both local and regional air quality and global climate change, such as carbon monoxide, methane, volatile organic compounds (VOCs), and the alternative chlorofluorocarbons. In addition, the OH radical initiates reactions that lead to the production of ozone in the atmosphere, the primary component of photochemical smog. Most of these reactions convert OH to both the hydroperoxy radical (HO_2) and organic peroxy radicals (RO_2),

ACPD

7, 12877–12926, 2007

which in the presence of nitrogen oxides (NO_x) are converted back to OH, resulting in a fast cycling of radicals that forms the basis of oxidation mechanisms in the atmosphere

Measurements of HO_x radicals (defined as OH + HO_2) can provide a critical test of current models of the fast photochemistry of the atmosphere (Heard and Pilling, 2003; Heard, 2006). However, because of its high reactivity, concentrations of OH in the troposphere range from less than 10^5 cm^{-3} at night in remote/rural environments (Tanner and Eisele, 1995; Bey et al., 1997), to greater than 10^7 cm^{-3} in urban environments (Ren et al., 2003a), with lifetimes less than one second. HO_2 radical concentrations are typically 5–100 times higher than OH (Stevens et al., 1997; Tan et al., 2001; Ren et al., 2003a; Ren et al., 2006). Only a few instruments are capable of making in-situ measurements of OH and HO_2 with the required sensitivity, low levels of interferences, and a temporal resolution that is fast enough to catch the rapid response of OH to external perturbations. Measurements of HO_x radicals are currently done using Differential Optical Absorption Spectroscopy (DOAS), laser-induced Fluorescence Assay by Gas Expansion (FAGE) and Chemical Ionization Mass Spectroscopy (CIMS) (Heard and Pilling, 2003). These instruments have been used for both ground-based and aircraft-based campaigns and have been employed for simultaneous measurements of other chemical species such as HO_2(FAGE, CIMS), RO_2+HO_2 (CIMS) and CH_2O, SO_2, naphthalene (DOAS)(Clemitshaw, 2004).

The DOAS technique does not require a calibration, as it is based on the Beer-Lambert law, and is employed to measure an average concentration of OH along a long path length. CIMS and FAGE instruments are used to perform local point measurements and require an external calibration to determine the instrumental sensitivity towards OH and to take into account potential radical losses through the sampling zone. A known concentration of OH must be generated in air at atmospheric pressure under various conditions of temperature and relative humidity with an apparatus that is portable enough to be used during field measurements. Table 1 is a compilation of the sophisticated OH sources which have been used for calibration purposes. Low pressure discharge techniques (I) and (II) are not suitable for calibration of tropospheric

ACPD
7, 12877–12926, 2007

EGU

instruments because they do not take into account potential radical losses during sampling at atmospheric pressure. However, these techniques are valuable to calibrate stratospheric instruments that measure OH at low ambient pressures. The UV photolysis of water-vapor (III) has been used extensively to calibrate both FAGE and CIMS instruments. The others approaches (IV, V and VI) have only been used occasionally due to their poorer accuracies and their more complex and cumbersome calibration procedures.

Given the difficulty in generating a known concentration of OH radicals, the use of a single calibration method is a main concern. The accuracy of the calibration factor must be confirmed by performing (i) inter-comparisons between instruments based on fundamentally different techniques and/or (ii) cross-calibrations of the same instrument with distinct calibration approaches. Unfortunately, there have been relatively few intercomparisons of HO_x measurement techniques (Heard and Pilling, 2003). Most of these intercomparisons have involved a DOAS instrument that is considered as a reference technique due to its self-calibration and its good accuracy (1σ=7%)(Heard and Pilling, 2003). Despite measuring on different spatial scales, intercomparisons involving long-path DOAS measurements and local point FAGE or CIMS measurements are generally in good agreement. It is worth mentioning that the recent intercomparison which took place at Forschungszentrum Julich allowed the most robust intercomparison between the DOAS and FAGE techniques by using the well controlled atmosphere inside the SAPHIR chamber (Schlosser et al., 2007). OH Measurements were performed on 9 days and an excellent linear correlation was observed between both techniques on 6 days (r^2=0.93), yielding a unity slope and a negligible intercept. However, the FAGE instrument measured a higher OH concentration than the DOAS instrument for the 3 remaining days. These recent studies give confidence regarding the calibration of OH instruments by the water-vapor UV-photolysis technique and the low level of interferences of each measurement technique; nevertheless more studies are necessary to ensure that the calibration of OH instruments is correctly performed.

To date, only a few studies have been conducted involving cross-calibrations on the same instrument. Tanner and Eisele (1995) performed calibrations of their early CIMS instrument using the photolysis of both water-vapor and ozone (Table 1). The calibration factors derived from both methods were different by approximately 20%, well within the stated uncertainties. Hard et al. (2002) calibrated their FAGE instrument by monitoring the loss of a hydrocarbon in a continuously stirred tank reactor and compared this method to the steady-state concentration of OH produced from the reaction of O_3 with trans-2-butene. The sensitivities derived from both techniques agreed within the stated uncertainties of each method (~37%). Bloss et al. (2004) validated the calibration of their FAGE instrument during experiments at the European photo-reactor (EUPHORE). The FAGE instrument, calibrated with the water-vapor UV-photolysis technique, was employed to measure the concentration of OH during the OH-initiated oxidation of aromatic compounds. The measured concentrations were compared to calculated concentrations inferred from measured hydrocarbon decays in the photo-reactor and good agreement was observed for 5 different aromatic species. Nevertheless a strong disagreement was found for 1,3,5-trimethylbenzene for which the measured and calculated OH concentrations differed by a factor of three.

The accuracy of in situ measurements of OH and HO_2 radicals in the atmosphere is critically dependent on the accuracy of the calibration method. This paper presents a detailed comparison of two different OH calibration techniques using the same FAGE instrument: the widely used water-vapor UV-photolysis technique and the steady-state ozone-alkene technique. The results of this study provide additional insights in the accuracy of these two OH calibration techniques.

2 Experimental section

2.1 IU-FAGE instrument description

The IU-FAGE instrument is based on the design of GTHOS (Ground-based Tropospheric Hydrogen Oxides Sensor) developed at Pennsylvania State University (Stevens et al., 1994; Mather et al., 1997; Faloona et al., 2004) and takes advantages of the detection of tropospheric OH by laser-induced fluorescence at low pressure using the Fluorescent Assay by Gas Expansion (FAGE) technique (Hard et al., 1984). Only a brief description is given here, a complete instrumental description will be provided in an upcoming publication (Dusanter et al., manuscript in preparation).

Unlike the GTHOS instrument, the current version of the IU-FAGE HO_x instrument uses a single axis for detection of both OH and HO_2 radicals. A schematic of the sampling cell is shown in Fig. 1. Air is pumped through a flat pinhole of approximately 1-mm diameter and is expanded through a cylindrical nozzle (5-cm diameter, 20-cm long) before the detection axis. Three mechanical vacuum pumps (Leybold D16B, 20 m^3h^{-1}) are connected in parallel to provide a flow rate of 9–10 SLPM through the sampling nozzle, allowing air to be refreshed rapidly at the detection axis. The internal pressure is maintained at 5.3±0.2 hPa and is monitored by an absolute capacitance gauge (MKS 0–13.3 hPa, better than 1% precision). The operating pressure was chosen for the following reasons: (i) an early FAGE instrument exhibited an unusual drop in sensitivity with an increase of the ambient water-vapor mixing ratio by operating the sampling cell at a lower pressure (Hofzumahaus et al., 1996; Creasey et al., 1997). This effect was attributed to radical scavenging on water cluster formed in the cold zone of the gas expansion. (ii) The sensitivity is strongly dependent on the operating pressure (Faloona et al., 2004); however, this dependence is minimized around 5.3 hPa and potential pressure changes during field measurements would induce less variation on the sensitivity than at other pressures.

A tunable dye laser (Lambda Physik, Scanmate 1) equipped with a BBO doubling crystal is pumped by a frequency-doubled Nd:YAG Laser (Spectra Physics Navigator II

YHP40-532Q) to generate radiation around 308 nm (~20 ns pulse width) at a repetition rate of 6 kHz and an averaged laser power of 1–15 mW. The laser power was found to be optimum by operating the dye laser with a mixture of Rhodamine 640 in isopropanol. The resulting laser light is transmitted inside the sampling cell by an optical fiber (2-m long, Thor Labs) and irradiates the sampled air mass through a multi-pass cell (24 passes, White design). Dry nitrogen is continuously flushed through each end of the optical cell to avoid a dead volume and to keep the mirrors clean.

The laser emission is adjusted on-resonance with the Q_1 Eq. (3) transition of OH at 308.1541 nm to promote a fraction of radicals from the ground state OH ($X^2\Pi$,v=0) to the first electronically excited state $OH^*(A^2\Sigma^+$, v=0). This transition was chosen because the Q_1 Eq. (3)-Q_{21} Eq. (3)-P_1 Eq. (1) triplet is easily identified and the Q_1 Eq. (3) transition exhibits one of the strongest absorption cross sections (σ=1.4×10^{-16} cm^2, P=1013 hPa, T= 300 K) around 308 nm (Dorn et al., 1995). In addition, a rapid switching between Q_1 Eq. (3) and P_1 Eq. (1) allows for a check for potential spectral interferences from other ambient species. The resonant fluorescence is collected by a gated detection system composed of a micro-channel plate (Hamamatsu R5916U-50), a preamplifier (F-100T, Advanced Research Instruments) and a time-gated photon counter (SRS400, Stanford Research). Electronic gating of the detector allows temporal filtering of the weak OH fluorescence from the much more intense scattered laser light.

The measurement of HO_2 is based on its rapid gas-phase reaction with nitric oxide as shown by Reaction (R1) and subsequent detection as OH. A small flow of pure NO (Matheson, better than 99% purity) is added through a loop injector located just below the inlet after passing though an ascarite trap. To convert most of the HO_2 radicals before the detection axis, the optimum flow rate (~1 SCCM) is a trade-off between the conversion of HO_2 into OH and the removal of OH by reaction with NO (R2); as a result, the fraction of HO_2 converted into OH must be determined by calibration.

$$HO_2 + NO \rightarrow OH + NO_2 \quad \text{(R1)}$$

ACPD
7, 12877–12926, 2007

EGU

$$OH + NO + M \rightarrow HONO + M \quad \text{(R2)}$$

Unknown impurities in the NO mixture can be photolyzed and interfere with HO_2 measurements by producing OH at high laser power. We recently observed an interference showing a quadratic dependence with the laser intensity and a linear dependence with the NO concentration, characteristic of a two-photon photolytic process. This interference has not been identified yet but has been quantified in laboratory and during field experiments (Dusanter et al., 2007).

The FAGE instrument is not a zero-background technique and the background signal, also called the off-resonance signal, must be measured to derive the net signal produced by the OH fluorescence. The procedure employed is based on successive modulation cycles during which the wavelength is successively tuned on-resonance and off-resonance with the Q_1Eq. (3) transition. During measurements, half the time is devoted to measure the off-resonance signal and the rest of the time is dedicated to measure the on-resonance signal. The net OH signal (S_{OH}) is inferred from the subtraction between the on-resonance signal and the two surrounding off-resonance signals. When NO is added to the sampled air stream, the sum (background + net OH + net HO_2) is measured. The net HO_2 signal (S_{HO2}) is derived from the subtraction between the net OH signal with NO added and the net OH signal without NO.

The radical concentrations are calculated by inverting Eqs. (1) and (2), and require the measurement of S_{OH}, S_{HO2} and the laser power P_w. It also requires the calibration of the detector response towards OH (R_{OH}) and HO_2 (R_{HO2}):

$$S_{OH} = [OH] \times R_{OH} \times P_W \quad (1)$$

$$S_{HO_2} = [HO_2] \times R_{HO_2} \times P_W \quad (2)$$

R_{OH} represent the number of photon counts per second produced per OH radical and normalized to 1-mW of laser power. R_{HO2} is the product of R_{OH} and the fraction of HO_2 converted into OH prior the detection axis ($R_{HO2}=R_{OH} \times C_{HO2}$).

The fluorescence quantum yield is dependant on collisional quenching which deexcites OH^* by inelastic scattering and consequently the sensitivity depends on operating conditions such as the pressure, the temperature and the chemical composition of the sampled air mass. The most efficient quenchers of OH^* in ambient air are N_2, O_2 and H_2O. The radiative lifetime of OH^* in dry air is 116-ns at 5.3 hPa and 298 K, almost 6 times shorter than its natural lifetime (Bailey et al., 1997). It is obvious that a change in the quenching rates of OH^* would result in a change of the instrumental sensitivity. However, constant atmospheric O_2 and N_2 mixing ratios as well as the well-stabilized internal pressure do not cause variation of the quenching rates. Water-vapor is known to be an efficient quencher of OH^*, more efficient than N_2 and O_2 at similar concentrations. As a result, the lifetime of OH^* decreases to 106-ns in air containing 1% of water-vapor, and the sensitivity of the IU-FAGE instrument is expected to decrease by approximately 13% per percent of water. The water mixing ratio is highly variable in the troposphere (1–3%) and care must be taken to calibrate the dependence of the OH response toward the water concentration.

The instrumental stability is largely governed by the stability of the laser intensity. Slow drifts are tracked during measurements by monitoring the laser power at the exit of both, the dye laser (UV_{dye}) and the white cell (UV_{cell}). The ratio UV_{cell}/UV_{dye} is used to track the transmission of the laser light through the optical fiber and the cleanliness of the optics inside the white cell. During instrument calibrations, the measurement precision depends on fluctuations of the background signal due to variations in laser scatter, and fluctuations of the OH concentration at the exit of the calibrator. The total uncertainty associated to a measured OH concentration also depends on the error introduced by the calibration technique, due to the inaccuracy of the quantities involved in the calculation of the OH concentration inside the calibrator. The systematic part of this error is time invariant and is usually larger than the measurement precision.

ACPD
7, 12877–12926, 2007

2.2 The water-vapor UV-photolysis calibration technique.

This technique takes advantage of direct photolysis of water-vapor at 184.9 nm in air and at atmospheric pressure. The photolysis of water leads to the production of an equal amount of OH radicals and H atoms (R3). The later are then stochiometrically converted into HO_2 on a sub-microsecond timescale by O_2 (R4):

$$H_2O + h\nu\,(184.9\text{nm}) \rightarrow OH + H \quad \text{(R3)}$$

$$H + O_2 + M \rightarrow HO_2 + M \quad \text{(R4)}$$

$$[OH]=[HO_2]=[H_2O]\times\sigma_{water}\times\Phi_{OH+H}\times(F\times t) \quad (3)$$

$$R_{OH}=\frac{S_{OH}}{[OH]\times P_W} \quad (4)$$

Equation (3) shows that the concentrations of OH and HO_2 are calculated from the time-integrated photolysis rate of water, using its known absorption cross-section σ_{water}, the unity photodissociation quantum yield Φ_{OH+H} (Sander et al., 2006), the photon flux (F) and the photolysis time (t). It is worth mentioning that the absorption cross section of water-vapor at 184.9 nm (σ_{water} $=7.14\times10^{-20}$ cm^2 $molecule^{-1}$) has been re-measured recently by several groups (Cantrell et al., 1997; Hofzumahaus et al., 1997; Creasey et al., 2000). The instrumental sensitivity R_{OH} is then determined by measuring the laser power and the net OH signal generated at the known OH concentration produced by the calibrator as shown in Eq. (4). During their transport inside the calibrator, the radicals can undergo chemical reactions and their sinks must be well understood to derive the right concentrations of OH and HO_2 entering the instrument. These radical loss reactions include self- and cross-reactions (R5–R7) as well as the radical losses on the wall of the apparatus (R8–R9):

$$OH + OH \rightarrow H_2O + O \quad \text{(R5)}$$

$$HO_2 + HO_2 \rightarrow H_2O_2 + O_2 \quad \text{(R6)}$$

ACPD
7, 12877–12926, 2007

EGU

$$OH + HO_2 \rightarrow H_2O + O_2 \quad \text{(R7)}$$

$$OH + \text{wall} \rightarrow \text{loss} \quad \text{(R8)}$$

$$HO_2 + \text{wall} \rightarrow \text{loss} \quad \text{(R9)}$$

To determine the contribution of homogeneous radical loss on the concentration of OH and HO_2 in the calibrator, the chemical system including Reactions (R5–R7) was modeled over the typical range of HO_x concentrations generated (1.1×10^9–1.5×10^{10} cm^{-3}) and a reaction time of 25–50 ms. The results show that radical losses coming from radical-radical reactions are mainly due to (R7), reducing the calculated concentration of OH and HO_2 from 1 to 9%.

In addition to water photolysis, molecular oxygen is photolyzed at 184.9 nm (R10) producing only ground-state atomic oxygen (Okabe, 1978):

$$O_2 + h\nu\,(184.9\,\text{nm}) \rightarrow O(^3P) + O(^3P) \quad \text{(R10)}$$

$$O_2 + O(^3P) + M \rightarrow O_3 + M \quad \text{(R11)}$$

$O(^3P)$ subsequently reacts with O_2 to form O_3 (R11), which can modify the partitioning between OH and HO_2 through reactions (R12–R13):

$$OH + O_3 \rightarrow HO_2 + O_2 \quad \text{(R12)}$$

$$HO_2 + O_3 \rightarrow OH + 2O_2 \quad \text{(R13)}$$

Adding these reactions to the model with an O_3 mixing ratio of 10 ppb (corresponding to the maximum observed during calibrations) affects the concentration of OH and HO_2 by less than 0.1%. However, care must be taken to perform calibration at a low concentration of O_3 in order to minimize secondary chemistry which could be catalyzed on the wall of the calibrator as suggested by Hard et al. (2002).

A low-pressure mercury lamp that emits at 184.9 nm but also at longer wavelengths is used as the photolysis source. From this lamp, the emission at 253.7 nm is about

ACPD
7, 12877–12926, 2007

EGU

8 times higher than that at 184.9 nm Schultz et al., 1995). Photolysis of ozone occurs at 253.7 nm and generates excited atomic oxygen that subsequently reacts with water-vapor and produces additional OH radicals. However, despite an ozone absorption cross section ~160 times higher at 253.7 nm than that for water at 184.9 nm, the low ozone mixing ratio generated during a calibration suggests that this source of OH is insignificant compared to the water photolysis process. Emissions at 184.9 and 253.7 nm also photolyses HO_2 and produces OH in the illuminated region with a photolysis frequency that is approximately 100 times higher than for H_2O (Sander et al., 2006). Nevertheless, as for O_3, the low mixing ratio of HO_2 makes this source of OH negligible. Emissions longer than 253.7 nm do not induce secondary photochemistry in the calibrator.

Both laminar (Creasey et al., 1997; Holland et al., 1998; Holland et al., 2003) and turbulent (Faloona et al., 2004) operating flow conditions have been used previously with the water-vapor UV-photolysis technique. Under laminar flow conditions, with Reynolds numbers below 2000, the flow is characterized by a radial velocity profile exhibiting the highest velocity at the center of the reactor where air is sampled by the instrument. As a result air in the center of the reactor has a shorter residence time in the illuminated region, leading to an OH concentration that is lower than that determined from Eq. (3) using the average velocity to calculate the photolysis time. The calculated OH concentration must be corrected by a factor which depends on the fraction of gas that is sampled by the instrument and how the laminar flow is developed (Creasey et al., 1997; Heard and Pilling, 2003). This approach has the advantage of low wall reactions, but requires an accurate determination of the correction factor.

Under turbulent flow conditions, where the Reynolds number is greater than 4000, the flow is characterized by a flat radial velocity profile due to turbulent mixing, and the OH concentration is uniformly distributed. The advantages compared to the laminar approach are twofold; there is no need to correct the calculated OH concentration due to different flow velocities, and the calibration is less sensitive to radial movement of the calibrator because the OH concentration is more uniform than for a laminar flow.

On the other hand, the turbulent flow induces a higher loss rate of the radicals on the wall, which must be measured.

The air exposure to the UV light, defined by the quantity (F×t) in Eq. (3), is required to calculate the OH and HO_2 concentrations. This quantity is difficult to quantify accurately, and two different approaches can be used to measure it experimentally: (i) absolute determinations of (F) and (t) separately, (ii) actinometric experiments to directly derive the product (F×t). The first approach requires an accurate characterization of the light source in terms of its photon flux distribution. The flux from the lamp at 184.9 nm must be mapped carefully and measured with a calibrated photodetector (Faloona et al., 2004). The measurement of the photon density must be highly selective at 184.9 nm and must be performed on a regular basis to catch the flux variations due to the aging of the lamp. Moreover, the light must be carefully collimated trough the calibrator to avoid potential reflections from the wall and to allow an accurate estimate of the photon flux and the photolysis time.

Two different actinometers are usually used in the second approach. As mentioned above, the emission at 184.9 nm also photolyses oxygen and leads to the production of ozone through Reactions (R10–R11). Its concentration is related to the product (F×t) as shown in Eqs. (5) and (6) using a photolysis quantum yield Φ_{O3}=2:

$$[O_3]=[O_2] \times \sigma_{O_2} \times \Phi_{O_3} \times (F \times t) \quad (5)$$

$$(F \times t)=\frac{[O_3]}{2[O_2]\sigma_{O_2}} \quad (6)$$

Thus, oxygen actinometry can easily be performed during the calibration by measuring the concentration of ozone in the air stream exiting the calibrator (Heard and Pilling, 2003; Holland et al., 2003). It is assumed that in turbulent flow conditions, the concentration of O_3 measured reflect an average of the O_3 production that occurred all along the photolysis path length. It is worth mentioning that for the actinometric approach, there is no need to carefully characterize the spatial distribution of the light and reflections from the reactor wall are not a concern. O_2 actinometry also allows the tracking

of instabilities in the lamp during the calibration that may result in large fluctuations of the light intensity. As a result, instabilities in the lamp flux due to changes in lamp temperature are less crucial for this approach than in the absolute determination of (F) and (t).

The concentration of O_3 produced during a calibration (2–10 ppb) can be measured with a commercial ozone monitor and $[O_2]$ is fixed by the air mixture. However, several previous studies have shown that the oxygen absorption cross section is dependent on operating conditions (O_2 column density, lamp current, cooling flow) and it is necessary to measure σ_{O2} for each calibration system (Hofzumahaus et al., 1997; Lanzendorf et al., 1997). For example, Hofzumahaus et al. (1997) observed a variation in the measured O_2 absorption cross section of approximately 27% between seven different mercury lamps. The mercury-lamp system dependence is the result of the overlap between several features of the highly structured absorption spectrum of O_2 (Schumann-Runge band) and the lineshape of the emission at 184.9 nm that depends on the operating conditions of the lamp due to line reversal (Lanzendorf et al., 1997) and potential fluorescence of the fused silica envelope (Cantrell et al., 1997).

The quantity (F×t) can also be derived from nitrous oxide actinometry during separate experiments in air (Edwards et al., 2003). The product (F×t) is calculated from Eq. (7) using the known kinetics parameters involved in Reactions (R14–R17) and from measurements of the amount of nitrogen oxides produced:

$$N_2O + h\nu\,(184.9\,\text{nm}) \rightarrow N_2 + O(^1D) \quad \text{(R14)}$$

$$N_2O + O(^1D) \rightarrow 2NO \quad \text{(R15a)}$$

$$N_2O + O(^1D) \rightarrow N_2 + O_2 \quad \text{(R15b)}$$

$$O(^1D) + N_2 \rightarrow O(^3P) \quad \text{(R16)}$$

$$O(^1D) + O_2 \rightarrow O(^3P) \quad \text{(R17)}$$

$$(F \times t) = \frac{(k_{15a} + k_{15b})[N_2O] + k_{16}[N_2] + k_{17}[O_2]}{2k_{15a}\sigma_{N_2O}[N_2O]^2}[NO_x] \quad (7)$$

The ground state atoms of oxygen generated by the quenching of $O(^1D)$ and by the photolysis of oxygen rapidly reacts with O_2 and produces O_3 that subsequently convert NO into NO_2 and care must be taken to measure the sum of NO and NO_2.

The calibrator design used in these experiments is shown in Fig. 2 and is based on the turbulent flow approach together with oxygen/nitrous oxide actinometry. It consists of a rectangular flow reactor made of aluminum (1.27×1.27×30-cm) and is equipped with a suprasil window on each side. The light source is a low-pressure mercury lamp (UVP Inc, model 11sc1) housed in an aluminum cartridge that is continuously purged with dry nitrogen to prevent light absorption by atmospheric gases. The flow of N_2 also helps to control the temperature of the lamp. The photolysis volume inside the calibrator is approximately 1.27-cm height and 0.6×4.0-cm wide. The lamp housing can be adjusted along the calibrator length to characterize the loss of radicals (R5–R9) by changing both the reaction time through the calibrator and the exposure time to the reactor wall.

The flow rate of air (zero grade, Indiana Oxygen) is regulated by two mass flow controllers (MKS, M100B) and passes through a chemical trap containing CARULITE to remove traces of carbon monoxide. The flow is adjusted to 50 SLPM in order to increase the Reynolds number up to 4300 and to insure that the OH instrument only samples air from the calibrator. Under rare occasions, the total flow rate was reduced to 30 SLPM but the detected OH signal was observed to be much more sensitive to movement of the calibrator and these calibrations were excluded of the final analysis. Measurements of the velocity profile at 50 SLPM using a pitot tube reveal that the velocity changes by approximately 8% between the center of the reactor and a radius of 3 mm. However, even if the velocity is slightly higher at the center, the turbulent mixing that occurs after the photolysis zone provides a uniform concentration of OH.

A variable fraction of the flow (~2–40%) is diverted through two bubblers containing high purity water (J. T. BAKER, ultra resi-analysed) to vary the water-vapor fraction, and is mixed back with the initial flow through 7 m of Teflon tubing before entering the calibrator. The water-vapor and ozone mixing ratios are monitored in the excess flow exiting the calibrator using commercial analyzers. Care is taken to verify that these monitors sample only air flowing through the calibrator. The water-vapor mixing ratio is measured by a LI-COR 6262 monitor based on IR absorption spectroscopy. This monitor is regularly calibrated against a dew point generator (LI-COR 610) and the uncertainty of the measurement is estimated to be ±2% (1σ). The ozone mixing ratio is monitored by a Teledyne 400E monitor based on UV absorption spectroscopy. The monitor is calibrated against a photometric O_3 calibrator (API, M401) and the uncertainty of the measurement is estimated to ±0.5 ppb (1σ) at the detection limit.

As mentioned above, the O_2 actinometry approach requires measuring the oxygen absorption cross-section at 184.9 nm under the same operating conditions as during an OH calibration. Measurements were performed in a cylindrical cell (10-cm long) made of Pyrex and equipped with two suprasil quartz windows. The low-pressure mercury lamp was mounted in the housing used during OH calibrations and was continuously purged with dry nitrogen. This housing was designed to use the light emitted by the side of the lamp. The beam was collimated through an optical train composed of a pinhole, a biconvex lens and an iris. The emission at 184.9 nm was isolated by two interference filters (FWHM=20 nm, Acton Research) located in the lamp housing and in front of the detector. The path length outside the cell was minimized and continuously flushed with dry N_2. The pressure inside the cell was monitored by an absolute capacitance gauge (MKS 0-1333 hPa, better than 1% precision). The intensity of the light was measured by an amplified photodiode UDT-555UV from OSI Optoelectronics. The monochromaticity of the UV light around 184.9 nm was checked by using a flow of nitrogen containing 26% of nitrous oxide that absorbs more than 99.9% of the photons at 184.9 nm and less than 0.1% at 253.7 nm. The experimental set-up and the procedure used to derive absorption cross sections were tested by measuring the well known

ACPD
7, 12877–12926, 2007

absorption cross section of N_2O at 184.9 nm. The value $\sigma_{N2O}=(1.37\pm0.11)\times10^{-19}$ cm^2 derived from several experiments is in good agreement with the recommended value of 1.43×10^{-19} cm^2 (Sander et al., 2006) and confirmed that our experimental set-up was appropriate to measure the absorption cross section of O_2.

For the oxygen absorption cross section measurements, a flow of N_2 containing various mixing ratios of oxygen (0–3.3%) was continuously passed through the cell at a total flow rate of 0.5–1.5 SLPM. The mixture composition was controlled by a combination of two mass flow controllers (MKS 1179A). The attenuation of the light at 184.9 nm was measured by rapid subtraction between successive measurements in pure N_2 and N_2/O_2 mixtures flowing through the cell. σ_{O2} was determined as a function of O_2 column density from the Beer-Lambert law and is shown in Fig. 3. The HO_x calibrations used synthetic air, corresponding to a column density of 6.1×10^{18} molecule/cm^2. An absorption cross section of $(1.21\pm0.12)\times10^{-20}$ cm^2 was derived at this O_2 column density from more than 100 individual measurements and used to calculate the product (F×t) from Eq. (6) during OH calibrations. It is worth mentioning that additional measurements were carried out with a lamp housing designed to select the light coming from the top of the lamp. The absorption cross sections measured were approximately 30% lower than those measured with the light coming from the side of the lamp, probably due to a higher degree of line reversal.

The light intensity was adjusted by varying the voltage supplied to the mercury lamp power supply. The light intensity at 184.9 nm decreased by a factor of approximately 5 when the voltage was adjusted from 120 to 30 V, while measurements of σ_{O2} resulted in variations of less than 2%. Moreover, the variations of S_{OH} and $[O_3]$ measured at constant water mixing ratios during OH calibrations were linear with the supplied voltage, indicating that the intensity of the light at 184.9 nm changes linearly with the voltage with negligible changes in the oxygen absorption cross section. These results agrees with the observations of Creasey et al. (2000) who found that variations in the measured O_2 absorption cross section were less than 2% when the lamp current was varied between 2.5–10 mA.

To minimize temperature changes in the emission of the lamp, a flow of N_2 was passed through the lamp housing. Although the overall intensity of the lamp decreased as the cooling flow was increased, measurements of σ_{O2} were independent of the cooling flow, suggesting that the oxygen absorption cross section measured for the mercury lamp used during these OH calibrations is not dependent on the lamp temperature. A second emission line from the mercury lamp at 194.2 nm can also contribute to the photolytic processes. Its emission intensity is about 2 orders of magnitude lower than the primary emission at 184.9 nm, but its intensity has been observed to increase as the temperature of the lamp decreased (Cantrell et al., 1997), in contrast to the observed decrease in the intensity at 184.9 nm. The absorption cross-section of water is about 2 orders of magnitude lower at 194.2 nm than at 184.9 nm (Creasey et al., 2000) and as a result the contribution of the second line to the water photolysis is negligible. More importantly, a change in the partitioning of photons between 184.9 and 194.2 nm could induce a change in the photolysis of O_2. However, measurements of σ_{O2} performed at various flow of N_2 through the lamp housing suggest that these changes are negligible under these operating conditions.

2.3 The steady-state ozone-alkene calibration technique

It is now well-established that the ozonolysis of alkenes is an important source of atmospheric radicals such as OH, HO_2 and RO_2 (Paulson and Orlando, 1996; Donahue et al., 1998). These reactions have also been proposed as a source for the calibration of OH instruments (Hard et al., 2002). In this technique, a steady-state concentration of OH is produced inside a flow-tube reactor by the ozonolysis of an alkene (R18):

$$O_3 + \text{alkene} \rightarrow \text{intermediates} \rightarrow \alpha_1 OH + \alpha_2 HO_2 + \Sigma \alpha_{P_i} P_i \quad \text{(R18)}$$

$$OH + \text{alkene} \rightarrow \text{products} \quad \text{(R19)}$$

$$OH + O_3 \rightarrow HO_2 + O_2 \quad \text{(R20)}$$

$$OH + \text{wall} \rightarrow \text{loss} \quad \text{(R21)}$$

The resulting OH radical can react with its precursors (R19–R20) as well as the wall of the reactor (R21). P_i designates any co-products of OH and HO_2 such as carbonyl species and thermalized Criegee intermediates (hereinafter referred to as TCIs). The competition between OH production and removal processes leads to the generation of a steady state concentration, which is calculated using Eq. (8) and the known kinetic parameters of (R18–R21):

$$[OH]_{SS} = \frac{k_{18}\alpha_1[O_3][\text{alkene}]}{k_{19}[\text{alkene}] + k_{20}[O_3] + k_{21}} \quad (8)$$

After expansion in the low pressure chamber of the FAGE instrument, the rates of the bimolecular reactions are divided by a factor equal to $(P_{atmosphere}/P_{IU-Fage})^2 \sim 36\,000$ at sea level. As a consequence, the secondary chemistry involving OH radicals occurring inside the sampling cell is negligible during the short transit-time to detection.

The validity of the steady-state equation is discussed by Hard et al. (2002) and only a brief summary is given here. Secondary chemistry occurring in the flow-tube, such as additional OH production and loss reactions, can limit the validity of Eq. (8). Products of reaction such as HO_2, carbonyl species and P_i, are produced by (R18) and the concentration of these species either build up in the system or reach a steady state until they can perturb the steady-state OH concentration (R13, R22–R24):

$$P_i + OH \rightarrow \text{products} \quad (R22)$$

$$P_i + O_3 \rightarrow \alpha_3 OH + \text{products} \quad (R23)$$

$$P_i + \text{alkene} \rightarrow \alpha_4 OH + \text{products} \quad (R24)$$

$$[O_3] \times t << \frac{\alpha_1}{\alpha_{P_i}\alpha_3 k_{23}} \quad (9)$$

$$[\text{Alkene}] \times t << \frac{\alpha_1}{\alpha_{P_i}\alpha_4 k_{24}} \quad (10)$$

ACPD
7, 12877–12926, 2007

EGU

Hard et al. (2002) have shown that secondary chemistry can be neglected when Eqs. (9) and (10) are satisfied. The right side of these equations has been estimated to be approximately 3.7×10^{15} molecule/cm^{3}s by assuming that P_i is a thermalized Criegee intermediate and $\alpha_{pi}=\alpha_3=\alpha_4=1$. The worst experimental conditions employed during our calibrations lead to maximum values of 2.5×10^{13} molecule/cm^{3}s for $[O_3]\times t$ and 2.6×10^{11} molecule/cm^{3}s for [alkene]×t, more than 2 order of magnitude below the upper limit.

The sensitivity of the instrument can be determined from rearranging Eqs. (1) and (8) into Eq. (11):

$$\frac{1}{S_{OH}} = b + m\frac{1}{[alkene]}; b=\frac{1}{R_{OH}K_{alkene}[O_3]P_W}; m=b\left(\frac{k_{21}+k_{20}[O_3]}{k_{19}}\right) \quad (11)$$

$$R_{OH}=\frac{1}{bK_{alkene}[O_3]P_W} \quad (12)$$

A calibration consists of measuring S_{OH} at various alkene concentrations for a constant ozone concentration. The parameter b is derived from the y-intercept of a linear regression of $1/S_{OH}$ versus 1/[alkene] and R_{OH} is calculated from Eq. (12). The advantage of using Eqs. (11) and (12) instead of Eqs. (8) and (4) is that the parameter b is independent of k_{20} and k_{21} and a change in the wall losses will not affect the calibration. K_{alkene} is a numerical constant defined by the known kinetic parameters of Reactions (R18) and (R19), $K_{alkene}=\alpha_1\times k_{18}/k_{19}$.

A close inspection of Eq. (8) shows that the procedure described above to determine R_{OH} could be simplified if the steady state concentration of OH is generated using a large concentration of alkene. Under these conditions, Eq. (8) simplifies to $[OH]_{ss}=K_{alkene}\times[O_3]$. $[OH]_{ss}$ is then independent of k_{20} and k_{21}, and R_{OH} can be derived from Eq. (4). However, in order for $k_{19}\times$ [alkene] $>10\times(k_{20}\times[O_3]+k_{21})$, the alkene concentration must be greater than 5×10^{12}molecule/cm^3 (assuming the alkene is trans-2-butene, an O_3 mixing ratio of a few ppm and $k_{21}=27\,s^{-1}$from Hard et al., 2002).

Hard et al. (2002) observed an interference during calibrations performed in dry air at high concentrations of trans-2-butene and excluded measurements at concentrations above 3×10^{12} molecule/cm^3 from their analysis. Moreover, using a high alkene concentration may allow (R18) to persist in the low-pressure cell of the FAGE instrument as mentioned by the same authors. For these reasons, we decided to derive R_{OH} from Eqs. (11) and (12).

We selected trans-2-butene (hereafter referred to as T2B) to calibrate the IU-FAGE instrument for several reasons. The OH yield reported from scavenger studies does not exhibit a pressure dependence for T2B in the range 27–1013 hPa (Fenske et al., 2000; Hard et al., 2002). Because R_{OH} is directly proportional to $1/K_{T2B}$ and given the large uncertainty associated to the rate constants at ambient temperature (Table 3), the calibration should be performed as close as possible to 298 K in order to avoid additional sources of uncertainty from the temperature dependence of the rate constants. This is a major drawback to using this calibration technique outside of the laboratory.

It has been argued that TCIs can undergo reactions with water-vapor (Neeb et al., 1997; Tobias and Ziemann, 2001), resulting in an OH yield that would depend on the water-vapor concentration. However, measurements performed during scavenger experiments have shown that the OH yield measured in dry and humid air for T2B are independent of the water concentration (Hasson et al., 2003). The pressure dependence and the reaction of the TCIs with water are discussed in detail in the Discussion section.

A schematic of the ozone-alkene apparatus is shown in Fig. 4, and consists of a cylindrical reactor (Pyrex, 1.27-cm diameter, 65-cm long) coupled with an internal injector (PTFE, 3-mm diameter). Reagent mixing is achieved by using an injector designed with radial holes and several Teflon coils, located upstream the mixing zone, to generate turbulences. Ozone is generated by photolysis of O_2 at 184.9 nm in a separate photolysis cell equipped with 2 low-pressure mercury lamps (UVP Inc, model 11sc1). A PTFE filter is connected downstream of the photolysis cell to scavenge any excited atomic oxygen produced by the photolysis of O_3 at 253.7 nm.

The air flow (zero grade, Indiana Oxygen) passes through a chemical trap containing Carulite and is regulated by a mass flow controller (MKS, M100B). The flow rate is adjusted in the range of 13–20 SLPM and is divided into two air streams. The first air stream supplies 5–20 SLPM of air to the O_3 photolysis cell, while the remainder passes through two water bubblers (J. T. Baker, ultra resi-analysed). Both air streams are mixed back together through 7 m of Teflon tubing before entering the flow-tube. A variable flow of T2B (30 ppm in N_2, Matheson, purity better than 95%) is adjusted in the range 0–20 SCCM by a mass flow controller (MKS, 1179A), and is added to the flow-tube through the injector. The total flow rates lead to Reynolds number between 1500 and 2400, characteristic of laminar-turbulent conditions. The averaged velocities result in reaction times in the range 140–210 ms, which are longer than the time required to reach the steady state (5–19 ms), and short enough to avoid secondary chemistry based on Eqs. (9) and (10). Pitot tube measurements performed at the exit of the flow-tube show that the velocity changes by about 24% between the center of the reactor and a radius of 3.5-mm.

A fraction of the O_3/water/air mixture introduced inside the flow-tube is continuously sampled by two commercial monitors to quantify the water-vapor and O_3 mixing ratios. The monitors used during these calibrations are the same as those employed for the water-vapor UV-photolysis calibration experiments. The uncertainties (1σ) of the measurements are ±2% for the water mixing ratio and ±5% for the O_3 measurement. Ozone and water-vapor mixing ratios generated during calibrations were typically in the range 1–4 ppm and 0–1.6% respectively. The OH wall loss rate was investigated by plotting m/b versus $[O_3]$ (see Eq. 11), resulting in a loss rate of approximately 20 s^{-1}.

ACPD
7, 12877–12926, 2007

3 Results

3.1 Water-vapor UV-photolysis calibration results

Typical OH calibrations are shown in Fig. 5 Panel (a). The high flow rate used in this technique generates turbulent conditions that produces a uniform concentration of radicals, but also increases radical loss. To quantify the loss of radicals, the residence time in the reactor was varied by changing the location of the light source on the calibrator. High losses were observed for OH, and its concentration was extrapolated at the exit of the calibrator by using a simple linear regression. The scatter in the signal observed in Panel (a) is typical of all the calibrations we performed to derive R_{OH} at a total flow rate of 50 SLPM and the precision (1σ) of the extrapolation is better than 4%. The total OH loss observed in our calibrator is on the order of 20–35% for a reaction time of 40-ms and increases slightly as the HO_x concentrations increase. Only 1–9% can be attributed to radical-radical reactions. This OH decay is attributed to wall losses that are much higher than that observed by Faloona et al. (2004) using a similar system. The high wall loss of OH is likely due to the fact that the walls of the calibrator are uncoated. In contrast, Panel (b) shows that HO_2 is less reactive than OH on the wall of the reactor and the HO_2 signal does not decrease as the residence time is increased. The extrapolated signals of OH and HO_2 are equal as expected from Eq. (3), suggesting that the conversion efficiency of HO_2 into OH is close to 100%. Future versions of the calibrator will be coated with Teflon in order to minimize these wall reactions.

The calibration results are shown in Fig. 6. The photolysis flux was varied to produce mixing ratios of O_3 over the range 2–10 ppb and the water-vapor mixing ratio was adjusted between 1000 and 5500 ppm, resulting in OH concentrations in the range 1.1×10^{9}–1.5×10^{10} cm^{-3}. The laser power was kept close to 1-mW to avoid saturation of the detector, and S_{OH} ranged from 800 to 5800 ct/s (the detector response is linear up to 15 000 ct/s). The uncertainty (1σ) of R_{OH} depends on the uncertainties stated in Table 2. Using O_2 actinometry to determine (F×t), the addition of the quoted uncertainties in quadrature yields an overall uncertainty of 17%. The fraction of HO_2 converted

into OH is derived from the ratio S_{HO2}/S_{OH} extrapolated to the exit of the calibrator. This ratio (C_{HO2}) is closed to unity and suggests a high conversion efficiency. The uncertainty (1σ) of C_{HO2} determined in Table 2 is 6.5% and the propagation of errors on $R_{HO2} = R_{OH} \times C_{HO2}$ provides an overall uncertainty of 18%.

The quantity (F×t) was also measured in separated experiment using the N_2O actinometry approach described above. In order to compare values derived from O_2 and N_2O actinometry, the procedure consisted of measuring successively the concentration of O_3 produced in a flow of 50 SLPM of air zero flowing through the calibrator and the concentrations of NO_x produced in the same air flow by adding 8% of nitrous oxide (Matheson, purity better than 99%). Care was taken to ensure that the total flow rate was the same for each experiment in order to keep the photolysis time constant. NO and NO_2 were monitored by a chemiluminescence analyzer (Teledyne, 200E), which was calibrated against a standard of NO generated by dynamic dilution of a NO mixture (Matheson, certified mixture ±5%). The rate constants used to derive (F×t) from Eq. (7) are displayed in Table 2. The absorption cross section of N_2O at 184.9 nm is large (σ_{N2O}=1.43×10^{-19} cm^2) (Sander et al., 2006), leading to an attenuation of approximately 30% of the light through the calibrator under these experimental conditions. As a result, the production of nitrogen oxides during N_2O actinometry does not reflect the overall photon flux absorbed during O_2 actinometry. To compare both actinometric techniques, (F×t) derived from the photolysis of N_2O was corrected from the light attenuation by taking into account the integration of the flux all over the photolysis path length and by assuming that the air mass is well mixed at the exit of the reactor.

Comparison between both techniques shows that the N_2O photolysis approach leads to a value for (F×t) that is consistently above the O_2 photolysis method by a factor 1.3 when (F×t) is derived from the recommended rate constants from Atkinson et al. (2004), and by a factor 1.5 for the recommended rate constants from Sander et al. (2006). However, this difference is within the uncertainties stated in Table 2, and these results give confidence in the characterization of the photon flux and the photolysis time performed with O_2 actinometry during OH calibrations.

3.2 Ozone-alkene calibration results

Two typical calibrations are shown in Fig. 7 and consist of successive measurements of the net OH signal at various alkene concentrations. S_{OH} is derived from the difference between the on-resonance signal and the average of the two surrounding off-resonance signals. The alkene concentration was increased for each on-resonance measurement, and was varied from 0 to 8.7×10^{11} molecule cm^{-3}. Inspection of Panel (a) in Fig. 7 shows that OH is not detected in dry air for the first on-resonance measurement when the added alkene concentration is zero. In contrast, Panel (b) shows that for the same measurement in humid air, a large signal of OH is observed. This signal was found to be linearly dependant on the O_3 and water concentrations and showed a quadratic dependence with the laser power, and is likely due to the well known O_3-water photolytic interference (Davis et al., 1981; Smith and Crosley, 1990). OH is produced inside the sampling cell through Reactions (R25–R26) by laser photodissociation of O_3 at 308-nm and subsequent reaction of $O(^1D)$ with water-vapor:

$$O_3 + h\nu\,(308\,\text{nm}) \rightarrow O(^1D) + O_2 \quad \text{(R25)}$$

$$O(^1D) + H_2O \rightarrow OH + OH \quad \text{(R26)}$$

$$O(^1D) + \text{T2B} \rightarrow OH + \text{products} \quad \text{(R27)}$$

The laser-generated OH is detected within the same laser pulse that produced it. The current set-up of the IU-FAGE instrument was found to be sensitive to this interference under the high concentrations of O_3 used in these calibrations, probably because of beam overlapping in the multi-reflection White cell.

The excited oxygen atoms produced from (R25) can also react with T2B (R27) as the bimolecular rate constants of (R26)(Dunlea and Ravishankara, 2004) and (R27)(Kajimoto and Fueno, 1979) are comparable. However, the maximum concentration of T2B used during these calibrations was below 10^{12} molecule/cm^3 and when a mixing ratio of water vapor as low as 0.1% is introduced inside the flow-tube, the rate

of (R26) becomes faster than (R27). Therefore the spurious OH coming from (R27) is negligible in moist air.

During calibrations, O_3 and water mixing ratios are kept constant and the signal arising from the laser-generated OH can be treated as an offset provided that the laser power does not drift on the short timescale of the experiment. As a result, S_{OH} recorded when [alkene]=0 was subtracted from the net OH signal measured when the alkene was present. The plateau reached by S_{OH} at large alkene concentrations in Panel (b) is consistent with Eq. (8), as the concentration of OH becomes independent of [T2B] and is equal to $K_{T2B} \times [O_3]$.

A close inspection of Panel (a) suggests that the plateau is not reached for calibrations performed in dry air, even at the highest alkene concentration. In addition, S_{OH} measured at the lowest alkene concentration (second on-resonance measurement) is relatively large. This behavior is likely a result of laser-generated OH from the reaction of $O(^1D)$ with T2B inside the detection cell that produces OH dependent on the alkene concentration (R27). As a consequence, calibrations performed in dry air can not be used to derive R_{OH} in the current configuration of the IU-FAGE instrument. However, improvement of the laser alignment in the multipass cell in order to minimize laser generated OH due to beam overlapping will allow calibration of the IU-FAGE instrument in dry air.

Plots of $1/S_{OH}$ versus [T2B] are presented in Fig. 8. R_{OH} was derived from the y-intercept (precision 1σ: 3–7%) and normalized to 1-mW of laser power. All calibrations performed are summarized in Fig. 6. These calibrations were performed at an ambient temperature of 30±2°C and K_{T2B} was corrected for the temperature dependence displayed in Table 3, although it induces a larger uncertainty on the rate constants k_{18} and k_{19}. The dependence of R_{OH} on the water-vapor concentration was fitted by a linear regression excluding R_{OH} measured in dry air. The sensitivity derived from the calibrations performed in dry air appears to be 12% higher than those performed in humid air and is consistent with the laser-generated source of OH discussed above that causes an overestimation of the sensitivity. The uncertainty (1σ) of R_{OH} depends on

ACPD
7, 12877–12926, 2007

the uncertainties quoted in Table 3, and the combined sources of errors give an overall uncertainty of 44% at 298 K.

4 Discussion

4.1 General considerations

Both calibration techniques exhibit similar advantages, such as the production of OH at atmospheric pressure, a homogeneous OH radial profile, good reproducibility, and are convenient to use during field measurements. For the water-vapor photolysis calibration scheme, no reaction rate constants are used and fewer associated uncertainties are involved in the calculation of the OH concentration. In addition, the OH signal measured during a calibration experiment is less sensitive to radial movements of the calibrator than the O_3-alkene technique, and the HO_2 conversion into OH can be quantified with the same apparatus. For the O_3-alkene calibration scheme, there is no need to measure photon flux and absorption cross sections, no need to check variations in the lamp spectral output, the laser generated OH from the O_3-water interference can be routinely checked and quantified during the calibration and OH can be produced in dry air, which is a significant advantage when the instrument need to be calibrated under ambient temperatures below 0°C. However, the increased uncertainty associated with the temperature dependence of the rate constants involved in the calculation of the steady-state OH concentration limits its use to temperature close to 298 K. Further kinetic studies are necessary to improve the accuracy of the required kinetic parameters at 298 K and their temperature dependences.

In the water-vapor photolysis approach, OH is generated in the nanosecond time scale. After generation, OH can only be removed by reactions with impurities present in the carrier gas and by wall reactions. This source is well suited for all types of OH instruments that require a calibration at atmospheric pressure. In contrast, for the steady-state O_3-alkene approach OH is continuously produced and consumed. This

technique is not suited to calibrate instruments such as the CIMS technique, where OH is converted into H_2SO_4 during the sampling stage because the O_3-alkene chemistry will continue to produce OH during the conversion step.

4.2 Intercomparison of absolute sensitivities and water-dependences

Figure 6 suggests that the absolute sensitivities derived from the O_3-alkene technique are approximately 40% lower than the water-vapor UV-photolysis technique. These results are similar to a comparison of the O_3-alkene technique that led to an averaged sensitivity that was approximately 11% lower than the CSTR technique (Hard et al., 2002) but contrast with an unpublished comparison that led to a good agreement between the water-vapor UV-photolysis and the steady-state O_3-alkene techniques (Heard and Pilling, 2003). Although within the uncertainties stated in Tables 2 and 3, the difference observed between the two calibration techniques used in this study is close to the 1σ values of their accuracies. Moreover, a recent study performed on the ozonolysis of short-chained alkenes (Wegener et al., 2007) suggests that the rate constant for the ozonolysis of T2B (k_{18} in Table 3) may be 1.2–1.3 times higher than the recommended value. Using this value to calculate K_{T2B} would decrease the sensitivities derived from the O_3-alkene technique by approximately 1.25 and would increase the difference between the two calibration techniques. These two points suggest a possible systematic error involved in one or both techniques.

One possible systematic error associated with the O_3-alkene calibration technique in these experiments may be the result of an OH production time-scale that is different for our calibration experiments compared to the scavenger experiments performed to derive the OH yield during T2B ozonolysis. The gas-phase ozone-alkene chemistry has been experimentally and theoretically investigated and the mechanism leading to the OH production is now well established (Fenske et al., 2000; Kroll et al., 2001a, 2001b; Hasson et al., 2003). Ozone adds across the double bond of an alkene to form an energy-rich primary ozonide (POZ) that rapidly dissociates into carbonyl species

ACPD
7, 12877–12926, 2007

and Criegee intermediates (CIs) as shown in Reaction (R28):

$$\text{alkene} + O_3 \rightarrow \text{POZ} \rightarrow \text{carbonyl} + \alpha_{CI^*}CI^* + (1-\alpha_{CI^*})\text{TCI} \quad \text{(R28)}$$

$$\text{syn}-CI^* \rightarrow \text{OH} + \text{R (prompt decomposition on a short timescale)} \quad \text{(R29)}$$

$$CI^* + M \rightarrow \text{TCI} + M \quad \text{(R30)}$$

$$\text{syn}-\text{TCI} \rightarrow \text{OH} + \text{R (thermal decomposition on a long timescale)} \quad \text{(R31)}$$

This reaction is highly exothermic (Gutbrod et al., 1996) and a fraction of the Criegee intermediates (α_{CI^*}) is formed with an excess of vibrational energy. The energy-rich CIs can undergo further unimolecular reactions and can form OH promptly (R29) or can be vibrationally stabilized by collisional quenching with the bath gas molecules (R30). Both, the energy rich CIs and the thermalized CIs (TCIs) can exist in the anti- or syn-configuration, with OH mainly produced from the decomposition of the syn isomer (Kroll et al., 2001b). The competition between the prompt decomposition to form OH and the collisional stabilization of the excited CIs leads to the pressure dependence of the OH yield observed at low pressure and short reaction times by Kroll et al. (2001a). At atmospheric pressure, collisional stabilization dominates relative to prompt decomposition and only a small fraction of the excited CIs decompose to produce OH.

Based on OH yield measurements performed at reaction times of 10–1000 ms and using time-dependent master equation calculations, Kroll et al. (2001b) suggested that the collisionally stabilized CIs can also produce OH by thermal dissociation (R31) but on a longer time scale than prompt decomposition. As a result, the O_3-alkene reactions exhibit a time-dependent OH yield, with a more pronounced effect at higher pressure. Moreover, it is believed that the vinoxy radical, formed as a coproduct of OH in Reactions (R29) and (R31), reacts with O_2 to form a chemically activated peroxy radical, which can isomerize and decompose to form OH (Kuwata et al., 2003). This secondary source of OH will also likely contribute to the time dependence of the OH yield.

As mentioned previously, the yield of OH employed to derive R_{OH} from the O_3-T2B calibration experiments has been inferred from scavenger studies (Atkinson and Aschmann, 1993; Fenske et al., 2000). These measured yields do not exhibit any pressure dependence, consistent with an OH production arising solely from the TCI decomposition. However, the timescale of these experiments (a few minutes) is much longer than the reaction time in the calibration flow-tube. As a result, the OH yield produced in the calibration system may be different than the OH yield derived from the scavenger studies (hereinafter referred as the global OH yield), that arises from the decomposition on a long time scale of both the TCIs and the vinoxy peroxy radical. Further studies on the time-dependence of the global OH yield are necessary to address this issue. However, one can speculate that if the yield of OH from the ozonolysis of T2B exhibits a similar time dependence as tetramethylethene (Kroll et al., 2001b), the OH yield at atmospheric pressure and ~140–210 ms of reaction time may be somewhat lower than the yield at longer reaction times. This would bring the absolute sensitivities derived from both calibration techniques into better agreement.

A close inspection of Fig. 6 shows that both calibration techniques do not exhibit an enhanced water-dependence as observed for an early FAGE instrument (Hofzumahaus et al., 1996). R_{OH} decreases by 20±10% (1σ) per percent of water for the water-vapor UV-photolysis technique and by 8±4% (1σ) for the O_3-alkene technique. Both calibration techniques exhibit water dependences that agree within their uncertainties. Taking into account the sampling conditions and the parameters of the time-gated detection for the IU-FAGE instrument, R_{OH} is expected to decrease by 13% per percent of water, in good agreement with that observed for both calibration techniques.

However, another potential error in the ozone-alkene calibration technique is the reaction of the TCIs with water-vapor. A competition between the thermal dissociation of the TCIs and their bimolecular reactions with water-vapor would affect the production of OH in the calibrator and the water dependence of R_{OH}. Anglada et al. (2002) performed quantum calculations on the reaction between water and the TCIs. They

pointed out that water-vapor may react with the TCIs to form a hydroxyalkyl hydroperoxide species (HAHP) (R32) with enough internal energy to undergo an O-O cleavage that leads to the production of OH (R33):

$$CH_3\dot{C}HO\dot{O} + H_2O \rightarrow [CH_3CH(OH)OOH]^* \quad \text{(R32)}$$

$$[CH_3CH(OH)OOH]^* \rightarrow CH_3CH(OH)\dot{O} + OH \quad \text{(R33)}$$

$$[CH_3CH(OH)OOH]^* + M \rightarrow CH_3CH(OH)OOH + M \quad \text{(R34)}$$

Master equation calculations performed by Hasson et al. (2003) indicate that the unimolecular decomposition of the chemically activated HAHP competes with its collisional stabilization (R34). As a result, OH production from the thermal dissociation of the syn-TCI may be lower in the presence of water-vapor. However, the anti-TCI may also react with water-vapor and produces a HAHP species, which could compensate the lower production of OH from the syn isomer.

These theoretical studies suggest that the OH yield for the ozonolysis of T2B may depend on the concentration of water vapor. A recent experimental study by Wegener et al. (2007) found an enhancement of the OH yield in the presence of water vapor during the ozonolysis of short-chained alkenes in the SAPHIR chamber. This study is in contrast with previous experiments performed on the ozonolysis of various alkenes in humid air by Neeb and Moortgat (1999), Johnston et al. (2001), Auschmann et al. (2002) and Hasson et al. (2003), which suggested that the presence of water does not affect the global OH yield. Clearly additional measurements of the water dependence of the OH yield from the ozonolysis of alkenes are needed to resolve these discrepancies.

However, the measurements of the OH yield for the ozonolysis of T2B by both Wegener et al. (2007) and Hasson et al. (2003) show no statistically significant dependence on water. This is consistent with the observed agreement between the water dependence of R_{OH} derived from the O_3-T2B and the water photolysis calibration discussed above. Nevertheless, the presence of water-vapor may have a stronger impact on calibrations performed using a different alkene as shown by the strong

ACPD
7, 12877–12926, 2007

OH yield enhancement observed for propene, 1-butene, isobutene and Cis-2-butene (Wegener et al., 2007).

4.3 Potential interferences in the calibration techniques

To determine whether the fluorescence of other species produced during the calibration may be interfering with the OH measurements, the fluorescence lifetime of OH^* was measured during calibration experiments. The fluorescence lifetimes observed for both techniques are similar, and agrees with the expected lifetime at 5.3 hPa. The fact that the sensitivity derived from the O_3-alkene calibration scheme is lower than from water UV-photolysis suggests that formation of OH from the decomposition of intermediates in the low-pressure region of FAGE is also negligible, although as mentioned above, it is possible that the effective OH yield at 140–210 ms of reaction time is somewhat lower than the yield derived from scavenger experiments.

Hard et al. (2002) observed an interference consistent with an additional OH source during calibrations of their FAGE instrument with the O_3-alkene technique. They determined that this interference was only present in dry air and for T2B concentrations above 3×10^{12} molecule/cm^3, higher than the concentrations used in this study. Interestingly, this interference was observed to disappear in moist air containing 1% of water-vapor, and tests were performed that ruled out the laser photolysis interferences described above. The authors suggested that this interference may be due to the dissociation of an intermediate in the low-pressure cell of their FAGE apparatus that results in the production of OH. We cannot rule out a similar interference in the O_3-T2B calibrations presented here, and this additional production of OH inside the low pressure region of the FAGE instrument would result in an overestimation of the sensitivity of the instrument. This potential interference requires further studies in order to assess whether intermediates generated during the ozonolysis of alkenes, as well as other atmospheric intermediates, decompose in the low-pressure region of the FAGE apparatus.

5 Conclusions

The overall goal of this study was to improve the confidence of current OH measurement techniques through an intercomparison of calibration techniques as a complement to instrument intercomparisons. Two different calibration techniques were used to accurately calibrate the IU-FAGE instrument. The first involved the photolytic dissociation of water-vapor at 184.9 nm and the second was based on the generation of a steady-state concentration of OH produced from ozone-alkene reactions. Both techniques were found to agree within their experimental uncertainties, although the sensitivities derived from the ozone-alkene technique were systematically lower than those derived from the water-vapor UV-photolysis technique. This suggests a systematic error, likely due the time dependence of the OH yield during O_3-alkene reactions. Because the timescale of OH generation in the ozone alkene calibration system is relatively short, the actual OH produced in the calibration system may be less than the global OH yield. The water-vapor UV-photolysis technique exhibits the highest accuracy and the lowest degree of secondary chemistry, and as a result, is the most suitable for calibrating OH instruments. Because several aspects of the mechanism of the gas-phase alkene ozonolysis are still uncertain, we recommend using the O_3-alkene calibration scheme only as a secondary method to derive the instrument response. Further studies are required to determine whether the recommended OH yield derived from scavenger experiments is suitable to calculate the steady-state concentration of OH generated at short reaction time in the ozone-alkene calibration systems containing water-vapor. In addition, unknown interferences associated with the ozone-alkene technique that could involve the decomposition of reaction intermediates at low pressure must be investigated. However, given the uncertainties associated with the ozone-alkene technique, the agreement between the two different methods improves the confidence of the water-vapor photolysis method as an accurate calibration technique for HO_x instruments.

Acknowledgements. We thank X. Ren and W. Brune for helpful discussions. This research is

supported by grants from the National Science Foundation (ATM-9984152 and 0612738) and the Camille and Henry Dreyfus Foundation.

References

Anglada, J. M., Aplincourt, P., Bofill, J. M., and Cremer, D.: Atmospheric formation of OH radicals and H_2O_2 from alkene ozonolysis under humid conditions, Chem. Phys. Chem., 2, 215–219, 2002.

Aschmann, S. M., Arey, J., and Atkinson, R.: OH radical formation from the gas-phase reactions of O_3 with a series of terpenes, Atmos. Env., 36, 4347–4355, 2002.

Atkinson, R.: J. Phys. Chem. Ref. Data, Monograph 1, 1989.

Atkinson, R. and Aschmann, S. M.: OH radical production from the gas-phase reactions of O_3 with a series of alkenes under atmospheric conditions, Environ. Sci. Technol., 27, 1357–1363, 1993.

Atkinson, R., Baulch, D. L., Cox, R. A., Crowley, J. N., Hampson, R. F., Hynes, R. G., Jenkin, M. E., Rossi, M. J., and Troe, J.: Evaluated kinetic and photochemical data for atmospheric chemistry: Volume I - gas phase reactions of O_x, HO_x, NO_x and SO_x species, Atmos. Chem. Phys., 4, 1461–1738, 2004, http://www.atmos-chem-phys.net/4/1461/2004/.

Bailey, A. E., Heard, D. E., Paul, P. H., and Pilling, M. J.: Collisional quenching of OH($A^2\Sigma^+$,v'=0) by N_2, O_2 and CO_2 between 204 and 294 K. Implications for atmospheric measurements of OH by laser-induced fluorescence, J. Chem. Soc., Faraday Trans., 93, 2915–2920, 1997.

Bey, I., Aumont, B., and Toupance, G.: The nighttime production of OH radicals in the continental troposphere, Geophys. Res. Lett., 24, 1067–1070, 1997.

Bloss, W. J., Lee, J. D., Bloss, C., Heard, D. E., Pilling, M. J., Wirtz, K., Martin-Reviejo, M., and Siese, M.: Validation of the calibration of a laser-induced fluorescence instrument for the measurement of OH radicals in the atmosphere, Atmos. Chem. Phys, 4, 571–583, 2004.

Calvert, J. G., Atkinson, R., Kerr, J. A., Madronich, S., Moortgat, G. K., Wallington, T. J., and Yarwood, G.: The mechanisms of atmospheric oxidation of the alkenes, Oxford University Press: New York, 2000.

Cantrell, C. A., Zimmer, A., and Tyndall, G. S.: Absorption cross sections for water vapor from 183 to 193 nm, Geophys. Res. Lett., 24, 2195–2198, 1997.

Clemitshaw, K. C.: A review of instrumentation and measurement techniques for ground-based

and airborne field studies of gas-phase tropospheric chemistry, Crit. Rev. Env. Sci. Tec., 34, 1–108, 2004.

Creasey, D. J., Halford-Maw, P. A., Heard, D. E., Pilling, M. J., and Whitaker, B. J.: Implementation and initial deployment of a field instrument for measurement of OH and HO_2 in the troposphere by laser-induced fluorescence, J. Chem. Soc., Faraday Trans., 93, 2907–2913, 1997.

Creasey, D. J., Heard, D. E., and Lee, J. D.: Absorption cross-section measurements of water vapour and oxygen at 185 nm. Implications for the calibration of field instruments to measure OH, HO_2 and RO_2 radicals, Geophys. Res. Lett., 27, 1651–1654, 2000.

Crutzen, P. J.: A discussion of the chemistry of some minor constituents in the stratosphere and troposphere, Pure Appl. Geophys., 106, 1385–1399, 1973.

Davis, D. D., Rodgers, M. O., Fischer, S. D., and Asai, K.: An experimental assessment of the O_3/H_2O interference problem in the detection of natural levels of OH via laser induced fluorescence, Geophys. Res. Lett., 8, 69–72, 1981.

Dilecce, G., Ambrico, P. F., and De Benedictis, S.: An ambient air RF low-pressure pulsed discharge as an OH source for LIF calibration, Plasma Sources Sci. Technol., 13, 237–244, 2004.

Donahue, N. M., Kroll, J. H., Anderson, J. G., and Demerjian, K. L.: Direct observation of OH production from the ozonolysis of olefins, Geophys. Res. Lett., 25, 59–62, 1998.

Dorn, H.-P., Neuroth, R., and Hofzumahaus, A.: Investigation of OH absorption cross sections of rotational transitions in the $A^2\Sigma^+$, v'=0 <– $X^2\Pi$, v"=0 band under atmospheric conditions: Implications for tropospheric long-path absorption measurements, J. Geophys. Res., 100, 7397–7409, 1995.

Dunlea, E. J. and Ravishankara, A. R.: Measurement of the rate coefficient for the reaction of $O(^1D)$ with H_2O and re-evaluation of the atmospheric OH production rate, Phys. Chem. Chem. Phys., 6, 3333–3340, 2004.

Edwards, G. D., Cantrell, C. A., Stephens, S., Hill, B., Goyea, O., Shetter, R. E., Mauldin, R. L., III, Kosciuch, E., Tanner, D. J., and Eisele, F. L.: Chemical Ionization Mass Spectrometer Instrument for the Measurement of Tropospheric HO_2 and RO_2, Anal. Chem., 75, 5317–5327, 2003.

Eisele, F. L. and Tanner, D. J.: Ion-assisted tropospheric OH measurements, J. Geophys. Res., 96, 9295–9308, 1991.

Faloona, I. C., Tan, D., Lesher, R. L., Hazen, N. L., Frame, C. L., Simpas, J. B., Harder, H., Mar-

tinez, M., Di Carlo, P., Ren, X., and Brune, W. H.: A Laser-Induced Fluorescence Instrument for Detecting Tropospheric OH and HO_2: Characteristics and Calibration, J. Atmos. Chem., 47, 139–167, 2004.
Fenske, J. D., Hasson, A. S., Paulson, S. E., Kuwata, K. T., Ho, A., and Houk, K. N.: The pressure dependence of the OH radical yield from ozone-alkene reactions, J. Phys. Chem. A, 104, 7821–7833, 2000.
George, L. A., Hard, T. M., and O'Brien, R. J.: Measurement of free radicals OH and HO_2 in Los Angeles smog, J. Geophys. Res., 104, 11 643, 1999.
Gutbrod, R., Schindler, R. N., Kraka, E., and Cremer, D.: Formation of OH radicals in the gas phase ozonolysis of alkenes: The unexpected role of carbonyl oxides, Chem. Phys. Lett., 252, 221–229, 1996.
Hard, T. M., O'Brien, R. J., Chan, C. Y., and Mehrabzadeh, A. A.: Tropospheric free radical determination by FAGE, Environ. Sci. Technol., 18, 768–777, 1984.
Hard, T. M., George, L. A., and O'Brien, R. J.: FAGE determination of tropospheric HO and HO_2, J. Atmos. Sci., 52, 3354–3371, 1995.
Hard, T. M., George, L. A., and O'Brien, R. J.: An Absolute Calibration for Gas-Phase Hydroxyl Measurements, Environ. Sci. Technol., 36, 1783–1790, 2002.
Hasson, A. S., Chung, M. Y., Kuwata, K. T., Converse, A. D., Krohn, D., and Paulson, S. E.: Reaction of Criegee intermediates with water vapor-An additional source of OH radicals in alkene ozonolysis?, J. Phys. Chem. A, 107, 6176–6182, 2003.
Heard, D. E. and Pilling, M. J.: Measurement of OH and HO_2 in the troposphere, Chem. Rev., 103, 5163–5198, 2003.
Heard, D. E.: Atmospheric field measurements of the hydroxyl radical using laser-induced fluorescence spectroscopy, Annu. Rev. Phys. Chem., 57, 191–216, 2006.
Hofzumahaus, A., Aschmutat, U., Heßling, M., Holland, F., and Ehhalt, D. H.: The measurement of tropospheric OH radicals by laser-induced fluorescence spectroscopy during the POPCORN field campaign, Geophys. Res. Lett., 23, 2541–2544, 1996.
Hofzumahaus, A., Brauers, T., Aschmutat, U., Brandenburger, U., Dorn, H.-P., Hausmann, M., Heßling, M., Holland, F., Plass-Dülmer, C., Sedlacek, M., Weber, M., and Ehhalt, D. H.: Reply, Geophys. Res. Lett., 24, 3039–3040, 1997.
Holland, F., Aschmutat, U., Heßling, M., Hofzumahaus, A., and Ehhalt, D. H.: Highly time resolved measurements of OH during POPCORN using laser-induced fluorescence spectroscopy, J. Atmos. Chem., 31, 205–225, 1998.

Holland, F., Hofzumahaus, A., Schäfer, J., Kraus, A., and Pätz, H.-W.: Measurements of OH and HO_2 radical concentrations and photolysis frequencies during BERLIOZ, J. Geophys. Res., 108, 8246, 2003.

Johnson, D., Lewin, A. G., and Marston, G.: The effect of Crieege-intermediate scavengers on the OH yield from the reaction of ozone with 2-methylbut-2-ene, J. Phys. Chem. A, 105, 2933–2935, 2001.

Kajimoto, O. and Fueno, T.: Relative rate constants of $O(^1D_2)$-Olefin reactions, Chem. Phys. Lett., 64, 445–447, 1979.

Kroll, J. H., Clarke, J. S., Donahue, N. M., Anderson, J. G., and Demerjian, K. L.: Mechanism of HO_x formation in the gas-phase ozone-alkene reaction. 1. Direct pressure-dependent measurements of prompt OH yields, J. Phys. Chem. A, 105, 1554–1560, 2001a.

Kroll, J. H., Sahay, S. R., Anderson, J. G., Demerjian, K. L., and Donahue, N. M.: Mechanism of HO_x formation in the gas-phase ozone-alkene reaction. 2. Prompt versus thermal dissociation of carbonyl oxides to form OH, J. Phys. Chem. A, 105, 4446–4457, 2001b.

Kuwata, K. T., Templeton, K. L., and Hasson, A. S.: Computational studies of the chemistry of syn acetaldehyde oxide, J. Phys. Chem. A, 107, 11 525–11 532, 2003.

Lanzendorf, E. J., Hanisco, T. F., Donahue, N. M., and Wennberg, P. O.: Comment on: "The measurement of tropospheric OH radicals by laser-induced fluorescence spectroscopy during the POPCORN field campaign" by Hofzumahaus et al. and "Intercomparison of tropospheric OH radical measurements by multiple folded long-path laser absorption and laser-induced fluorescence" by Brauers et al., Geophys. Res. Lett., 24, 3037–3038, 1997.

Levy, H.: Photochemistry of the lower troposhere, Planet. Space Sci., 20, 919–935, 1972.

Mather, J. H., Stevens, P. S., and Brune, W. H.: OH and HO_2 measurements using laser-induced fluorescence, J. Geophys. Res., 102, 6427–6436, 1997.

Matsumi, Y., Kono, M., Ichikawa, T., Takahashi, K., and Kondo, Y.: Laser-Induced Fluorescence instrument for the detection of tropospheric OH radicals, Bull. Chem. Soc. Jpn., 75, 711–717, 2002.

Neeb, P., Sauer, F., Horie, O., and Moortgat, G. K.: Formation of hydroxymethyl hydroperoxide and formic acide in alkene ozonolysis in the presence of water vapour, Atmos. Env., 31, 1417–1423, 1997.

Neeb, P. and Moortgat, G. K.: Formation of OH radicals in the gas-phase reaction of propene, isobutene and isoprene with O_3: Yields and mechanistic implications, J. Phys. Chem. A, 103, 9003–9012, 1999.

Okabe, H.: Photochemistry of small molecules, John Wiley & Sons, New York, 1978.
Paulson, S. E. and Orlando, J. J.: The reactions of ozone with alkenes: An important source of HO_x in the boundary layer, Geophys. Res. Lett., 23, 3727–3730, 1996.
Ren, X., Harder, H., Martinez, M., Lesher, R. L., Oliger, A., Shirley, T., Adams, J., Simpas, J. B., and Brune, W. H.: HO_x concentrations and OH reactivity observations in New York City during PMTACS-NY2001, Atmos. Environ., 37, 3627–3637, 2003a.
Ren, X., Harder, H., Martinez, M., Lesher, R. L., Oliger, A., Simpas, J. B., Brune, W. H., Schwab, J. J., Demerjian, K. L., He, Y., Zhou, X., and Gao, H.: OH and HO_2 Chemistry in the urban atmosphere of New York City, Atmos. Environ., 37, 3639–3651, 2003b.
Ren, X., Brune, W. H., Oliger, A., Metcalf, A. R., Simpas, J. B., Shirley, T., Schwab, J. J., Bai, C., Roychowdhury, U., Li, Y., Cai, C., Demerjian, K. L., He, Y., Zhou, X., Gao, H., and Hou, J.: OH, HO_2, and OH reactivity during the PMTACS-NY Whiteface Mountain 2002 campaign: Observations and model comparison, J. Geophys. Res., 111, D10S03, doi:1029/2005JD006126, 2006.
Sander, S. P., Friedl, R. R., Golden, D. M., Kurylo, M. J., Moortgat, G. K., Wine, P. H., Ravishankara, A. R., Kolb, C. E., Molina, M. J., Finlayson-Pitts, B. J., Huie, R. E., and Orkin, V. L.: Chemical kinetics and photochemical data for use in atmospheric studies, Evaluation number 15, JPL Publication 06-2, NASA Jet Propulsion Laboratory, Pasadena, California, 2006.
Schlosser, E., Bohn, B., Brauers, T., Dorn, H.-P., Fuchs, H., Häseler, R., Hofzumahaus, A., Holland, F., Rohrer, F., Rupp, L., Siese, M., Tillmann, R., and Wahner, A.: Intercomparaison of two hydroxyl radical measurement techniques at the atmosphere simulation chamber SAPHIR, J. Atmos. Chem., 56, 187–205, 2007.
Schultz, M., Heitlinger, M., Mihelcic, D., and Volz-Thomas, A.: Calibration source for peroxy radicals with built-in actinometry using H_2O and O_2 photolysis at 185 nm, J. Geophys. Res., 100, 18 811–18 816, 1995.
Smith, G. P. and Crosley, D. R.: A photochemical model of ozone interference effects in laser detection of troposheric OH, J. Geophys. Res., 95, 16 427–16 442, 1990.
Smith, S. C., Lee, J. D., Bloss, W. J., Johnson, G. P., Ingham, T., and Heard, D. E.: Concentrations of OH and HO_2 radicals during NAMBLEX: measurements and steady state analysis, Atmos. Chem. Phys, 6, 1435–1453, 2006.
Stevens, P. S., Mather, J. H., and Brune, W. H.: Measurements of tropospheric OH and HO_2 by laser-induced fluorescence at low pressure, J. Geophys. Res., 99, 3543–3557, 1994.

Stevens, P. S., Mather, J. H., Brune, W. H., Eisele, F. L., Tanner, D., Jefferson, A., Cantrell, C., Shetter, R., Sewall, S., Fried, A., Henry, B., Williams, E., Baumann, K., Goldan, P., and Kuster, W.: HO_2/OH and RO_2/HO_2 ratios during the tropospheric OH photochemistry experiment: Measurement and theory, J. Geophys. Res., 102, 6379–6391, 1997.

Tan, D., Faloona, I., Simpas, J. B., Brune, W., Shepson, P. B., Couch, T. L., Sumner, A. L., Carroll, M. A., Thornberry, T., Apel, E., Riemer, D., and Stockwell, W.: HO_x budgets in a decidious forest: Results from the PROPHET summer 1998 campaign, J. Geophys. Res., 106, 24 407–24 427, 2001.

Tanner, D. J. and Eisele, F. L.: Present OH measurement limits and associated uncertainties, J. Geophys. Res., 100, 2883–2892, 1995.

Tobias, H. J. and Ziemann, P. J.: Kinetics of the gas-phase reactions of alcohols, aldehydes, carboxylic acids, and water with the C13 stabilized Criegee intermediate formed from ozonolysis of 1-tetradecene, J. Phys. Chem. A, 105, 6129–6135, 2001.

Wegener, R., Brauers, T., Koppmann, R., Rodriguez Bares, S., Rohrer, F., Tillmann, R., Wahner, A., Hansel, A., and Wisthaler, A.: Simulation chamber investigation of the reactions of ozone with short -chained alkenes, J. Geophys. Res., 112, doi:10.1029/2006JD007531, 2007.

Table 1. Techniques employed to calibrate OH instruments.

Calibration techniques		Principle	Uncertainty (1σ)	Generated radicals	Laboratory/Field (drawbacks)	References
(I)	Low-pressure flow-tube RF discharge	H atoms are produced by a microwave discharge in a low-pressure flow tube. OH radicals are produced by titration of the H atoms with NO_2.	30%	OH	Laboratory (low ambient pressure calibration)	(Stevens et al., 1994)
(II)	Pulsed N_2-H_2O RF discharge	OH and NO are produced at low pressure with a low power RF discharge. The OH density is related to the NO density in the discharge.	20%	OH	Laboratory (low ambient pressure calibration, require measuring NO by LIF)	(Dilecce et al., 2004)
(III)	Water UV-photolysis	See experimental section.	10–30%	OH, HO_2	Laboratory / field (Photon flux measurements, lamp dependent absorption)	(Tanner and Eisele, 1995; Creasey et al., 1997; Holland et al., 1998; Matsumi et al., 2002; Heard and Pilling, 2003; Holland et al., 2003; Ren et al., 2003b; Faloona et al., 2004; Smith et al., 2006)
(IV)	steady-state O_3-alkene	See experimental section.	42%	OH	Laboratory/field (time consuming)	(Hard et al., 2002; Heard and Pilling, 2003)
(V)	Continuously Stirred Tank Reactor (CSTR)	OH is produced in a CSTR by UV-irradiation of an Hydrocarbon/H_2O/NO mixture. The OH concentration is calculated from the loss of the hydrocarbon.	36%	OH	Laboratory/field (bulky, time consuming, potential gradient of OH near the wall of the reactor)	(Hard et al., 1995; George et al., 1999; Hard et al., 2002)
(VI)	Laser photolysis of O_3	Ozone is photolysed at 248 nm and OH is produced by subsequent reaction of excited atomic oxygen with water. $O_3+h\nu \rightarrow O(^1D)+O_2$	40–50%	OH	Laboratory (bulky, expensive)	(Eisele and Tanner, 1991; Tanner and Eisele, 1995)

ACPD
7, 12877–12926, 2007

EGU

Table 2. Experimental conditions and uncertainties involved in the water-vapor UV-photolysis calibration technique.

Parameters	Value[a] (min/max)	Uncertainty (1σ %)
[OH] calculated from Eq. (3)	1.1×10^{9}–1.5×10^{10} cm^{-3}	15.5
$[H_2O]$	0.10–0.55 %	2
$\sigma_{water,185\,nm}$	7.14×10^{-20} cm^{-2}	3
Φ_{OH}	1	<1
O_2 Actinometry (Fxt)	4.1×10^{11}–2.1×10^{12} photon/cm^2	15
$[O_3]$	2–10 ppb	12
$[O_2]$	21%	5
$\sigma_{O2,185nm}$	1.21×10^{-20} cm^{-2}	10
N_2O Actinometry (Fxt)	1.7×10^{12} photon/cm^2	55/33
$[N_2O]$	7–8 %	5
$[NO_x]$	8–9 ppb	10
$\sigma_{N2O,185nm}$	1.43×10^{-19} cm^{-2}	2
Φ_{N2O}	1	<1
k_{15a}	7.2×10^{-11} / 6.7×10^{-11}	26 / 15
k_{15b}	4.4×10^{-11} / 5.0×10^{-11}	26 / 15
k_{16}	2.6×10^{-11} / 3.1×10^{-11}	26 / 10
k_{17}	4.0×10^{-11} / 4.0×10^{-11}	12 / 10
HO_2 conversion ($C_{HO2}=S_{HO2}/S_{OH}$)	1.02	6.5
S_{OH}	800–5800 ct/s	4
S_{HO2}	2900–6800 ct/s	5
F_{NO}	1 SCCM	1
$R_{OH}=S_{OH}/[OH]\times P_w$	7.2×10^{-7}–9.1×10^{-7} ct/s/cm^{-3}/mW	17
P_w	1 mW	5
$R_{HO2}=R_{OH}\times C_{HO2}$	7.2×10^{-7}–9.1×10^{-7} ct/s/cm^{-3}/mW	18

[a]Values and uncertainties on chemical rate constants are given for T=298 K and units for bi-molecular rate constants are in cm^3 molecule^{-1} s^{-1}. The first number is the value recommended by Atkinson et al. (2004) and the second number by Sander et al. (2006).

ACPD
7, 12877–12926, 2007

Table 3. Experimental conditions and uncertainties involved in the steady-state O_3-alkene calibration technique.

Parameters	Value[a] (min/max)	Uncertainty (1σ %)
K_{T2B}	$4.2\times10^{-4}e^{-1609/T}$	43
α_1	0.64	15
k_{18}	$6.6\times10^{-15}e^{-1059/T}$	35
k_{19}	$1.0\times10^{-11}e^{550/T}$	20
$R_{OH} = 1 / (b\times K_{T2B}\times[O_3]\times P_w)$	$3.9\text{x}10^{-7}$–$5.3\text{x}10^{-7}$ ct/s/cm^{-3}/mW	44
Intercept (b)	3.2×10^{-3}–4.5×10^{-4} (ct/s)$^{-1}$	7
$[O_3]$	1–4 ppm	5
P_w	1 mW	5

[a]Values and uncertainties on chemical rate constants are given for T=298 K and units for bimolecular rate constants are in cm^3 molecule^{-1} s^{-1}. k_{18} is the value recommended Calvert et al. (2000) and k_{19} is from Atkinson (1989). References for α_1 have been reviewed by Hard et al. (2002)

ACPD
7, 12877–12926, 2007

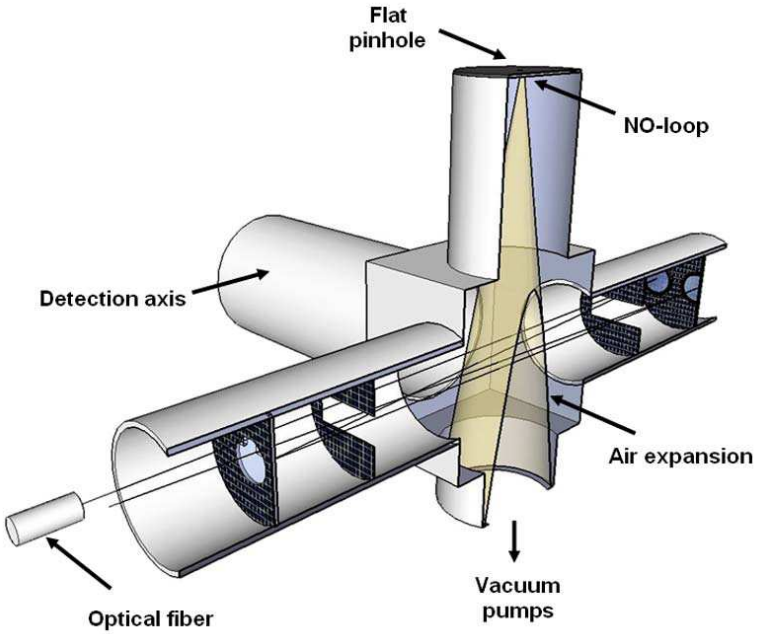

Fig. 1. Cross-section of the IU-FAGE detection cell. The flow controller and the Teflon loop used to regulate and mix the NO flow inside the sampled air stream are not displayed.

ACPD
7, 12877–12926, 2007

EGU

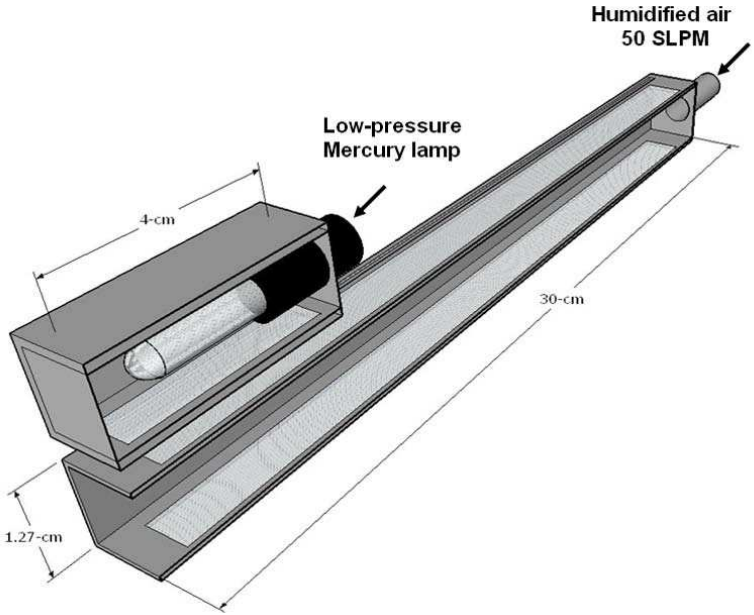

Fig. 2. Cross-section of the calibrator based on the water-vapor UV-photolysis technique.

ACPD
7, 12877–12926, 2007

EGU

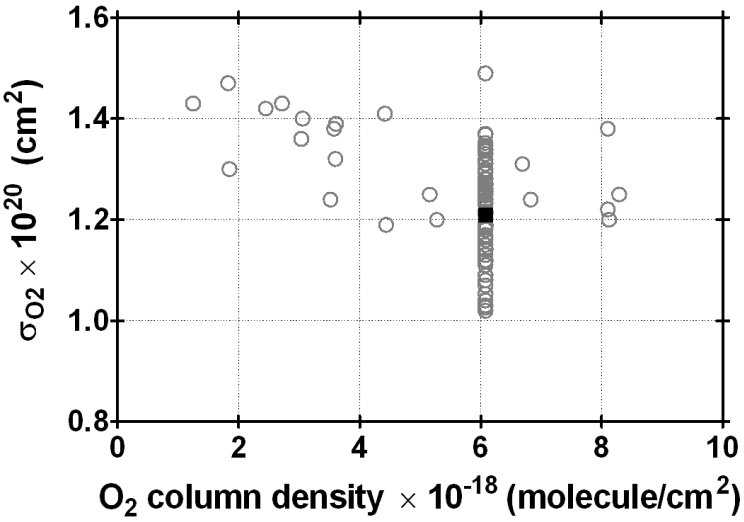

Fig. 3. Oxygen absorption cross-sections measured as a function of O_2 column density. The grey circles are individual measurements performed at various conditions of lamp temperatures and voltages. The dark square is an average of 101 measurements performed at a typical O_2 column density of 6.1×10^{-18} molecule/cm^2 used during OH calibrations. The average leads to $\sigma_{O2} = 1.21\times10^{-20}$ cm^2 with a standard deviation of 0.8%.

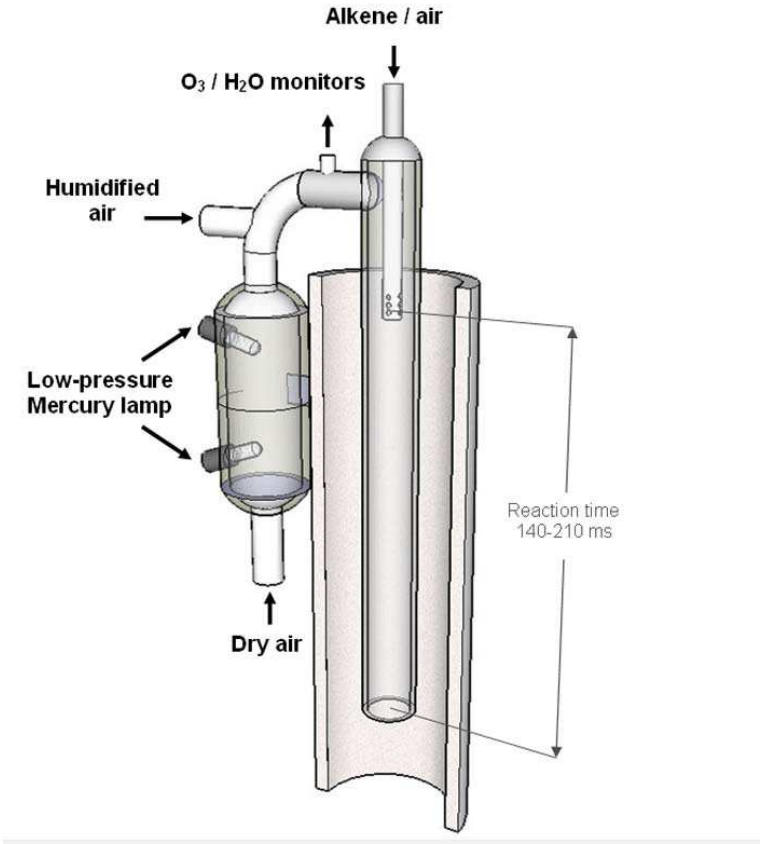

Fig. 4. Schematic of the calibrator based on the steady-state O_3-alkene technique.

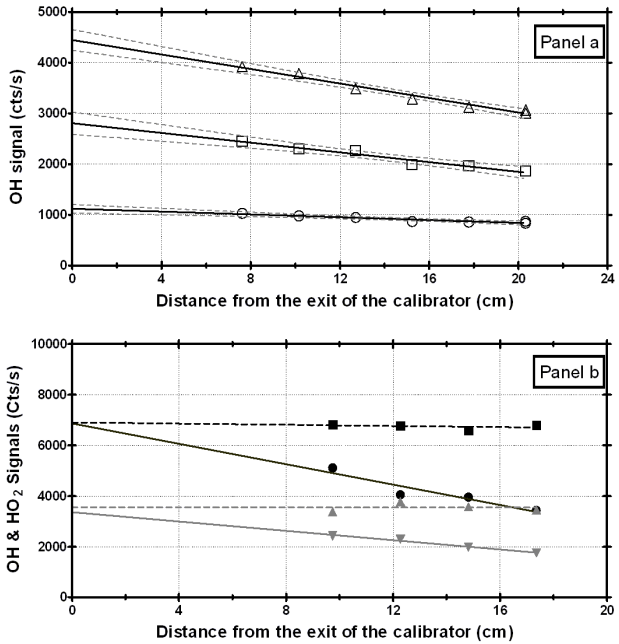

Fig. 5. Typical water-vapor UV-photolysis calibrations. OH and HO_2 signals are shown as a function of the distance between the exit of the calibrator and the radical productions. Panel a: calibrations performed at a total flow rate of 50 SLPM. Run 1: ∘[OH]=1.1×10^9 cm^{-3}; Run 2: □[OH]=3.7×10^9 cm^{-3}; Run 3: Δ[OH]=5.1×10^9 cm^{-3}. The dashed lines are the 95% confidence intervals of the linear regressions. Panel b: calibrations performed at a total flow rate of 30 SLPM. Run 1: •[OH] and ■[HO_2]=1.5×10^{10} cm^{-3}; Run 2: ▲[OH] and ▼[HO_2]=3.2×10^9 cm^{-3}.

ACPD
7, 12877–12926, 2007

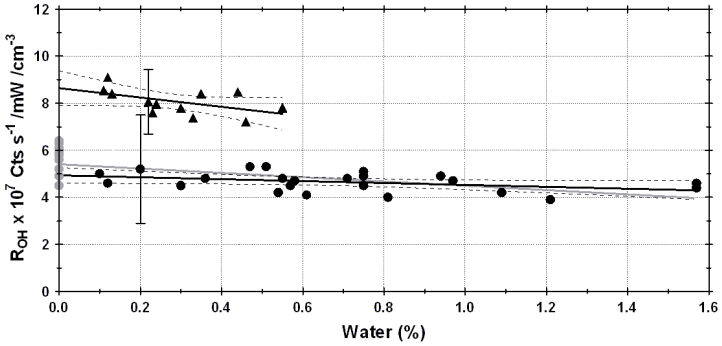

Fig. 6. Plot of R_{OH} versus $[H_2O]$. ▲ and • represent the respective sensitivities measured with the water-vapor UV-photolysis technique and the steady-state O_3-alkene technique. The dashed lines are the 95% confidence intervals of the linear regression. The error bars are the total uncertainty (1σ) stated in Table 1 and 3. The grey dots represent the points at $[H_2O]$= 0 from the calibrations performed with the steady-state O_3-alkene technique that have been performed in dry air.

ACPD
7, 12877–12926, 2007

EGU

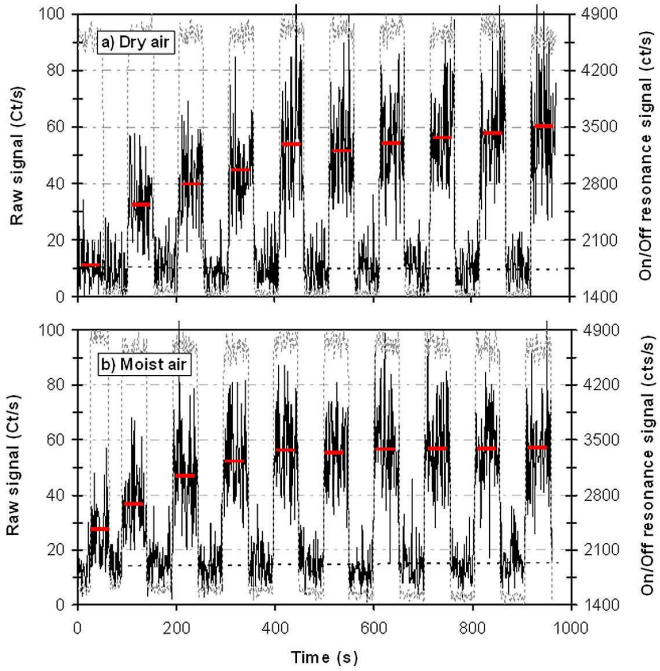

Fig. 7. Typical steady-state O_3-alkene calibrations. Panel a: calibration performed in dry air at 2.5 ppm of O_3. Panel b: calibration performed in humid air (0.75% of water) at 2.1 ppm of O_3. The grey dashed line indicates the modulation cycle used for the measurement of the on- and off-resonance signals. The solid black line is the recorded signal and the dashed black line is the average of all the off-resonance measurements. The first on-resonance measurement was acquired without alkene then [alkene] increases at each on-resonance measurements and is varied from 1.7×10^{11} to 8.7×10^{11} molecule cm^{-3}.

ACPD
7, 12877–12926, 2007

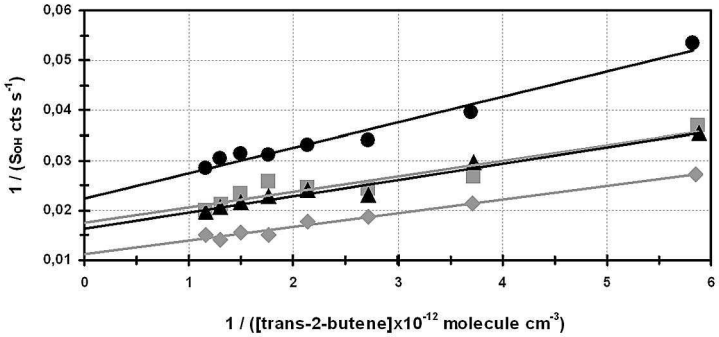

Fig. 8. Plot of $1/S_{OH}$ versus 1/[trans-2-butene] for 4 independent calibrations at various [O_3], [water] and laser power: •2.1 ppm O_3, 0.75% water, 1.0 mW; ■2.2 ppm O_3, 0.47% water, 1.0 mW; ▲2.5 ppm O_3, 0% water, 0.9 mW; ◇2.4 ppm O_3, 0% water, 1.4 mW.

ACPD
7, 12877–12926, 2007